JOURNAL OF PROPULSION AND POWER
Vol. 24, No. 2, March–April 2008

Flush-Wall, Diamond-Shaped Fuel Injector for High Mach Number Scramjets

Peter M. Grossman,* Luca Maddalena,* and Joseph A. Schetz†
Virginia Polytechnic Institute and State University, Blacksburg, Virginia 24061-0203

DOI: 10.2514/1.29956

Experiments on diamond-shaped injectors with sonic injection of heated helium into a nominal Mach 4 airflow are reported. The slender diamond was angled up 60 deg from the wall. These conditions correspond to a Mach 10 scramjet with helium to simulate hydrogen fuel. The diamond was tested at jet-to-freestream momentum flux ratios, $\bar{q}$, of 1.04 and 0.49, aligned with the freestream and with 15 deg yaw. For comparison, round injectors angled up 30 deg from the wall with $\bar{q} = 1.75$ were also examined. Previous studies have shown that diamond and round injectors each perform best at different values of $\bar{q}$. A sampling probe was used for helium concentration with Pitot, cone-static, and total temperature probes for other flow properties. For $\bar{q} = 1.04$, the diamonds penetrated about 50% higher than the round injector and produced a 30% wider jet. The diamonds exhibited 10–15% lower mixing efficiency. The total pressure loss parameter of the aligned diamond was 22% lower, while the yaw angle improved the total pressure loss parameter to 34% lower than the round injector. For the lower $\bar{q}$ case, the diamond demonstrated 52% higher penetration and a 39% wider plume than the round injector, and the mixing efficiency was only 4% lower. The total pressure loss parameter was 32% lower than the round injector. These results confirm earlier, lower Mach number and heavier injectant studies that a slender diamond injector provides significant benefits for penetration and lower total pressure losses.

Nomenclature

A	=	area
α	=	mass fraction
c_p	=	constant pressure specific heat
c_v	=	constant volume specific heat
f	=	stoichiometric hydrogen–air ratio
G	=	mass flow rate
γ	=	ratio of specific heats
η	=	combustor efficiency
η_m	=	mixing efficiency
M	=	Mach number
p	=	(static) pressure
p_c	=	cone static pressure
p_t	=	total pressure
$p_{t,\text{Pitot}}$	=	Pitot total pressure
$p_{t,\text{rec}}$	=	total pressure recovery factor
Π	=	total pressure loss parameter
$\bar{q}$	=	jet-to-freestream momentum flux ratio
R	=	gas constant
Re	=	Reynolds number
R_b	=	effective radius
ρ	=	density
T	=	temperature
u	=	flow velocity
V	=	voltage
x	=	axial distance downstream of injector center
y	=	lateral distance from the injector
$y^{\pm}$	=	plume width
z	=	vertical distance from the wall
z^{+}	=	plume center of mass height

Subscripts

j	=	jet exit property
s	=	system
t	=	total condition
∞	=	freestream property

I. Introduction

BECAUSE to the of very high freestream velocity of scramjets reaching Mach 10, fuel residence time is on the order of milliseconds [1], and supersonic combustion presents an interesting challenge in scramjet engines. It is, therefore, desirable to enhance penetration and mixing of the fuel plume to accomplish rapid combustion. Rapid combustion will produce an increase of combustion efficiency and a reduction of the required combustor length thus reducing the skin-friction drag and heat transfer and increasing the net thrust. To improve the overall engine efficiency, the injection process must also induce low total pressure losses. Jet injector enhancement in high-speed flows also has applications in other fields such as thermal protection systems and vehicle control by jet thrusters.

Many injector configurations have been studied by various groups in an attempt to produce enhanced mixing and penetration in wall injectors. Some of these configurations can be seen in Fig. 1 including swept ramps [1–10], slot injectors [11,12], transverse injection [13–18], and jet swirl [19–24]. An extensive review of injector mixing characteristics is given in Schetz et al. [25]. The focus of the current investigation is single-hole, flush-walled injectors. Flush-walled injectors are preferred over in-stream injectors because they minimize total pressure losses and heating. Single-hole injectors produce a counter-rotating vortex pair [26] when they interact with the freestream crossflow. This counter-rotating vortex pair is the major method of mixing enhancement in these injectors.

One of the more successful studies in further enhancing jet flow penetration in single-hole injectors was the use of a wedge-shaped hole with a rounded back introduced by Barber et al. [14]. The wedge-shaped front of the hole mitigated boundary layer separation upstream of the jet resulting in higher penetration compared with round injectors. The major drawback of the wedge injector design was that separation still occurred downstream of the injector due to the rounded back. Tomioka et al. [13] showed that replacing the round back of the injector hole with a rear-facing wedge would help

Received 23 January 2007; revision received 11 April 2007; accepted for publication 5 July 2007.

*Graduate Research Assistant, Aerospace and Ocean Engineering Department. Student Member AIAA.
†Holder of the Fred D. Durham Chair, Aerospace and Ocean Engineering Department. Fellow AIAA.

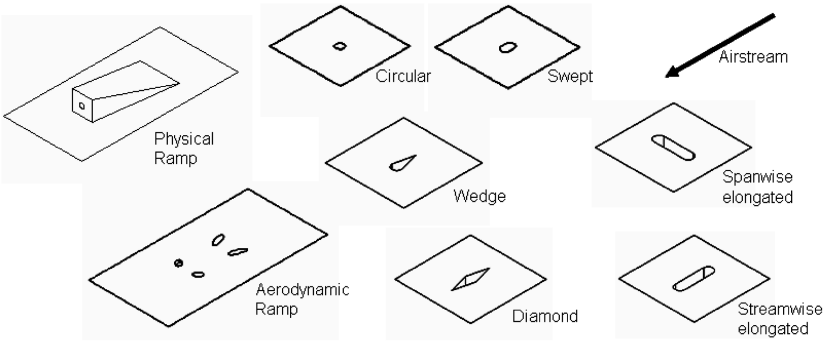

Fig. 1 Examples of various injector configurations.

to negate this problem. In addition, Tomioka, et al [13] showed that the addition of a moderate yaw angle to the diamond-shaped injector further enhanced penetration and mixing. It is suggested that this phenomenon is due to the fact that the yawed diamond shape in a crossflow acts like a pitched up airfoil, creating suction on one side and compression on the other, inducing a span-wise flow from the compression to the suction side. When this span-wise flow interacts with the counter-rotating vortex pair, streamwise vorticity is enhanced, increasing penetration.

The purpose of the present research is to determine the effectiveness of a diamond injector design that was initially proposed by Tomioka et al. [13] for $M = 3$ airflow with heated air injectant now in a nominal Mach 4 airflow with heated helium injectant. The diamond injector was tested both aligned with the freestream flow and at a 15 deg yaw angle and compared with a low-angled, circular injector investigated by Maddalena et al. [1] at the same nominal Mach 4 cross-stream conditions and mass-flow rate. This comparison is intended to verify the effectiveness at nominal Mach 4 conditions of injector configurations that have been previously proven successful at lower Mach number conditions with simulated hydrocarbon injectants. The nominal Mach 4 flow simulates conditions a scramjet combustor would encounter in Mach 10 flight. Heated helium was used to safely simulate hydrogen.

II. Experimental Setup

A. Test Facility

These experiments were conducted in the Virginia Polytechnic Institute and State University's blow-down type supersonic wind tunnel shown in Fig. 2.

The supersonic wind tunnel setup for these experiments used a converging–diverging nozzle to achieve a nominal Mach 4 flow in the test section. Flow conditions involved total pressure and temperature in the plenum chamber of $P_{t,\text{plenum}} = 1034$ kPa and $T_{t,\text{plenum}} = 295$ K. However, there was a weak oblique shock observed at the end of the nozzle, where the floor plate attached resulting in actual freestream conditions of Mach number $M_\infty = 3.8$, total pressure $P_{t,\infty} = 1029$ kPa, and total temperature $T_{t,\infty} = 295$ K at the injection station.

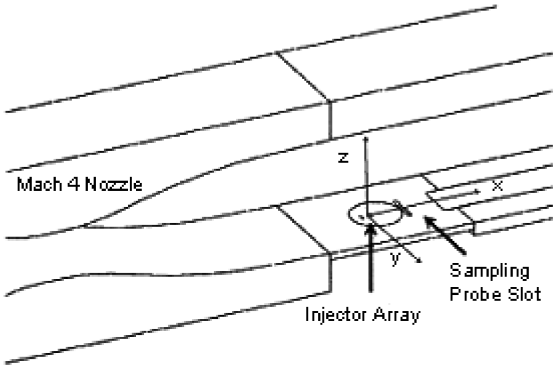

Fig. 2 Test arrangement in the Virginia Polytechnic Institute and State University supersonic wind tunnel.

B. Data Acquisition

Data from the experiments were acquired using a 16-channel, 16-bit A/D converter. A 64-channel multiplexer with a built-in cold-junction compensator was used for temperature measurements with a sampling rate of 500 Hz. *Labview* was used both to control the wind tunnel, traverse system, and injection and to collect data from the measurement probes

C. Injectors

Heated helium was used in these experiments to safely simulate hydrogen fuel in a scramjet engine. The helium was heated to a value of approximately 313 K by a flow heater in the feedline before the injector measurement devices and orifice.

When comparing injectors, it is important to normalize data to provide an objective and accurate comparison. Often, injector diameter is used to normalize lengths for round injectors of varying sizes. For injector arrays such as aeroramp injectors, equivalent diameter (the diameter of a single round injector with the same area as the total area of the injectors in the array) is employed. However, when comparing injectors of different shapes, equivalent diameter is a poor length scale, because changing injection properties can affect some shapes differently than others. Thus, a different length scale must be developed. The length scale used in these experiments is the effective radius R_b, defined as follows [14]:

$$R_b = \sqrt{\frac{G_j}{\rho_\infty u_\infty}} \tag{1}$$

To fully describe injector conditions, another parameter is used called the jet-to-freestream momentum flux ratio $\bar{q}$, defined as follows:

$$\bar{q} = \frac{(\rho u^2)_j}{(\rho u^2)_\infty} = \frac{(p\gamma M^2)_j}{(p\gamma M^2)_\infty} \tag{2}$$

1. *Round Injectors*

Conventional, round injectors were used as comparators. The baseline round injector in these experiments had a diameter of 3.226 mm, and it was angled 30 deg up from the wall as shown in Fig. 3. This injector was studied by Maddalena et al. [1] in the same facilities at the same conditions. The baseline case used a mass flow of 3.4 g/s for an effective radius of $R_b = 3.54$ mm and a jet-to-freestream total pressure ratio of 0.55 resulting in a jet-to-freestream momentum flux ratio of $\bar{q} = 1.75$. Values of $\bar{q}$ in this range and angles near 30 deg have been found to be near optimum for round injectors [25].

To provide a round injector comparison for the lower $\bar{q}$ diamond case described below, it was necessary to test another round injector with the same mass flow ($G_j = 1.5$ g/s) and effective radius ($R_b = 2.35$ mm) as the lower $\bar{q}$ diamond injector. To retain the same jet-to-freestream momentum flux ratio ($\bar{q} = 1.75$) as the baseline

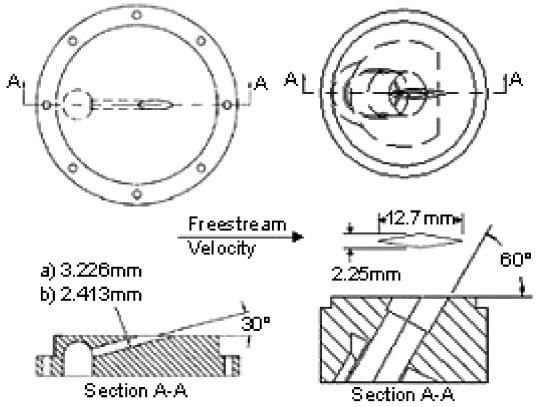

Fig. 3 Round injector insert (left) and diamond injector insert (right): a) baseline case, b) lower mass-flow case.

round injector, it was necessary to create a smaller round injector with a diameter of 2.41 mm and a jet-to-freestream total pressure ratio of 0.33.

2. Diamond Injector

The major injector configuration studied in these experiments was the diamond-shaped injector, which can be seen in Fig. 3. The diamond had a long dimension of 12.7 mm and a short dimension of 2.25 mm and was angled 60 deg up from the wall (in the long direction). The 60 deg angle was chosen in an attempt to maximize penetration. Initially, this injector was used with flow conditions set to match the mass flow of the baseline case round injector of 3.4 g/s. To achieve this mass flow, the jet-to-freestream total pressure ratio was 0.30 resulting in a jet-to-freestream momentum flux ratio of $\bar{q} = 1.04$ and an effective radius of $R_b = 3.54$ mm (matching the baseline case). A lower $\bar{q}$ is desirable for the diamond because if $\bar{q}$ becomes too high, the jet can rapidly plume outward losing the diamond shape and its benefits [13]. The diamond baseline case was tested both with the long dimension aligned with the freestream and at a 15 deg yaw angle. Yaw was achieved by simply rotating the diamond injector insert shown on the right in Fig. 3. The schlieren photograph in Fig. 4 shows the bow shock off the front of the injector, and the injection plume can be seen. The boundary curving up to the right is the edge of the window.

The diamond injector was also tested at an even lower $\bar{q}$ based on the work of Tomioka et al. [13]. This research indicated that a jet-to-freestream momentum flux ratio of about $\bar{q} = 0.5$ is near optimal for a diamond injector of this aspect ratio [13]. To achieve $\bar{q} = 0.49$ for this diamond, a jet-to-freestream total pressure ratio of 0.13 was required resulting in a mass flow of 1.5 g/s and an effective radius of $R_b = 2.35$ mm.

The injectors and conditions studied are summarized in Table 1.

3. Injection System

The helium injection system used two bottles of compressed helium, a dome pressure regulator, two total pressure transducers, a differential pressure transducer, two thermocouples, and a gasline heater.

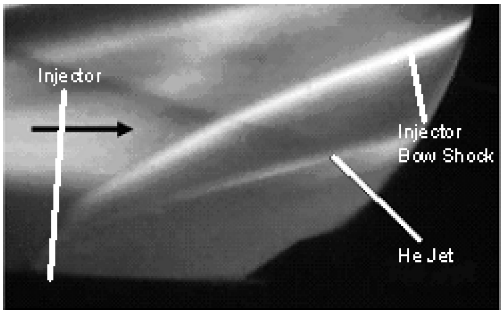

Fig. 4 Schlieren photograph of helium injector in crossflow.

Table 1 Injector summary

Shape	Size, mm	Injection angle	Yaw angle	G_j g/s	$\bar{q}$	R_b, mm
Round	3.23 diameters	30	0	3.4	1.75	3.54
Round	2.41 diameters	30	0	1.5	1.75	2.35
Diamond	12.7 × 2.25	60	0	3.4	1.04	3.54
Diamond	12.7 × 2.25	60	15	3.4	1.04	3.54
Diamond	12.7 × 2.25	60	0	1.5	0.49	2.35

The first total pressure transducer and type E thermocouple with the differential pressure transducer were placed in the line before the heater to measure the mass flow with a commercial Venturi flowmeter. The helium was then routed through the heater. The heated helium then passed the second pressure transducer and a type E thermocouple in the line just before the injector insert to measure the injection conditions.

III. Instrumentation

Injection plume measurements were taken at a vertical plane normal to the freestream flow direction 53 mm aft of the injector. This plane corresponds to a normalized distance of 15.0 R_b downstream of the baseline injectors and 22.5 R_b downstream of the lower mass-flow injectors. A Cartesian coordinate system was used with its origin on the wind tunnel floor along the test section centerline. The positive x-axis was aligned with the freestream direction, the positive z-axis was in the vertical direction up from the floor and the y-axis was aligned with the tunnel span direction.

All measurements in these experiments were accomplished using probes mounted on a vertical traversing system and inserted through slots cut in the wind tunnel floor as shown in Fig. 5. This setup was used to acquire data for a single vertical profile for each probe for one wind tunnel run. The probe span-wise position was adjusted manually between runs. To produce a full profile at the measurement plane, a vertical profile was taken at each of 13 equally-spaced span-wise stations over a distance of 38 mm. The uncertainty in the probe position was ±0.3 mm in the span-wise direction and ±0.2 mm in the vertical direction.

A. Species Composition Probing

Mean helium concentration measurements were accomplished using an integrated concentration sampling probe and gas analyzer designed for supersonic flow. The conceptual design of this type of probe was originally developed by Ng et al. [27]. The probe was aspirated during data acquisition by a vacuum pump. The concentration probe was calibrated to measure a unique helium mass fraction for a specific pressure, temperature and heat transfer rate at the hot-film sensor plane. Complete details are available in [28].

A file was generated showing the probe position, voltage, total pressure and total temperature for each wind tunnel run. For each probe position, a computer algorithm using these measurements was used to determine the upper and lower bounds on voltage for any calibration level. The program then searched iteratively for the two helium concentration calibration curves which bounded the voltage at the measured pressure and temperature. Then, the local helium

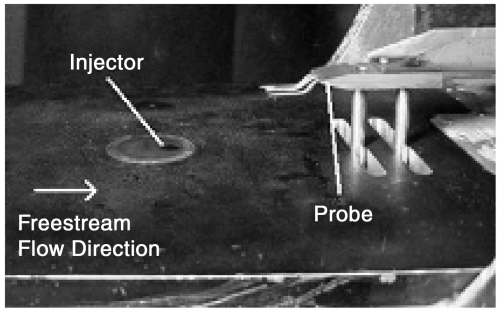

Fig. 5 Test setup showing injector and triple-probe rake.

concentration was interpolated between the two bounding curves. These algorithms are shown in [28]. The probe was found to have an uncertainty of approximately ±3% for helium mass fraction measurements.

B. Aerothermodynamic Probing

Aerothermodynamic measurements were taken with a triple-rake probe which included a Pitot pressure probe, a cone-static pressure probe and a total temperature probe as seen in Fig. 5.

These measurements along with the helium concentration were used with a combination of the Rayleigh-Pitot formula and a numerical solution of the Taylor–Maccoll equation to determine the local Mach number and total pressure at each sampling location. The uncertainty on the pressure measurements was ±6 kPa. The algorithms used to complete these calculations can be found in full in Ref. [28]. All other flow properties were then found using the perfect gas relations. All calculations assumed a calorically perfect gas, i.e., constant specific heats.

The total temperature was measured directly by the total temperature probe because total temperature remains constant across a normal shock. The uncertainty on the temperature measurements was ±2 K.

IV. Results and Analysis

A. Baseline Cases

This section discusses the total temperature, total pressure and concentration (mass fraction) data for the injectors using a mass flow of $G_j = 3.4$ g/s corresponding to an effective radius R_b of 3.54 mm. The results for the aligned and yawed diamond were compared to the baseline round injector. All plots in this section were taken from the measurement plane $15.0R_b$ downstream of the injectors. The plots extend to $\pm 5.35R_b$ in the span-wise direction and from 0 to $7.65R_b$ in the vertical direction.

1. Total Temperature Contours

Figure 6 shows the total temperature contours for the baseline mass-flow cases. The local total temperature values in the plots are normalized by the freestream total temperature of approximately $T_{t,\infty} = 295$ K. All three profiles are set to the same nondimensional scale for comparison. A qualitative and somewhat quantitative assessment of the injector behaviors can be obtained from the isothermal profiles.

The total temperature profiles for all three injector configurations show an arch-shaped structure, which is often demonstrative of the presence of a counter-rotating vortex pair. The counter-rotating vortex pair is present in most single-hole injectors in a supersonic crossflow, and it is the main mechanism for mixing enhancement and penetration for single-hole injectors.

The total temperature contours show a cooler core, a warmer exterior, and a more gradual temperature gradient in the round injector than the diamond injectors, which display a well-bounded hot core with a rapid drop off to the freestream total temperature at the edge of the arch structures. One must use caution in interpreting temperatures for mixing due to the Ranque-Hilsch effect. This effect states that total temperature is variable within a vortex structure, rendering the temperature analogy for mixing inconclusive.

2. Total Pressure Contours and Total Pressure Loss Parameter

Figure 7 shows the total pressure contours for the baseline mass-flow cases. The local total pressure values in the plots are normalized by the freestream total pressure of approximately $p_{t,\infty} = 1029$ kPa. All three profiles are set to the same nondimensional scale for comparison. Pressure losses from the air and fuel can be generated by viscous forces in the boundary layer, flow separation, shock waves, and/or fuel–air mixing.

The total pressure profiles indicate that the diamond injectors generate slightly higher local total pressure losses over a larger area than the round injector. However, the overall average total pressure losses are more revealing for injector performance than local observations. The overall total pressure loss is quantified using a total

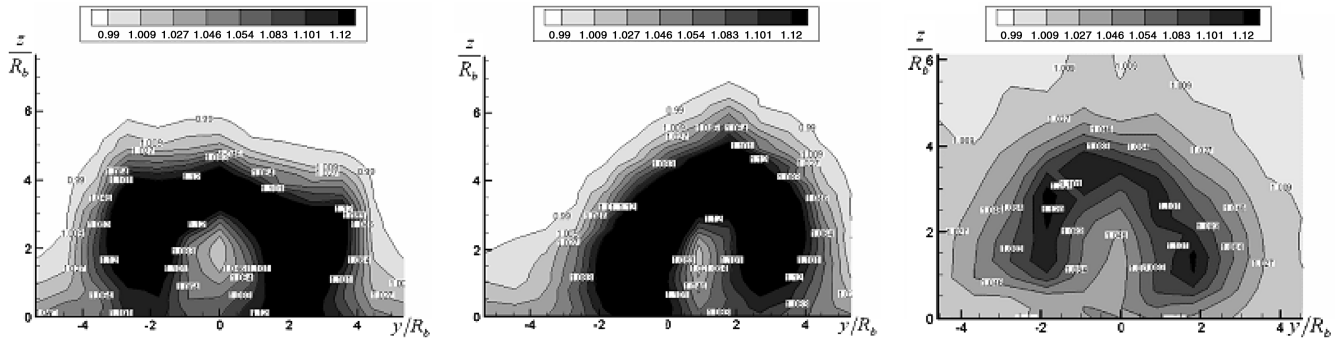

Fig. 6 Normalized total temperature contours $T_t/T_{t,\infty}$ for baseline case (left), aligned diamond injector (middle), and yawed diamond injector (right) round injector.

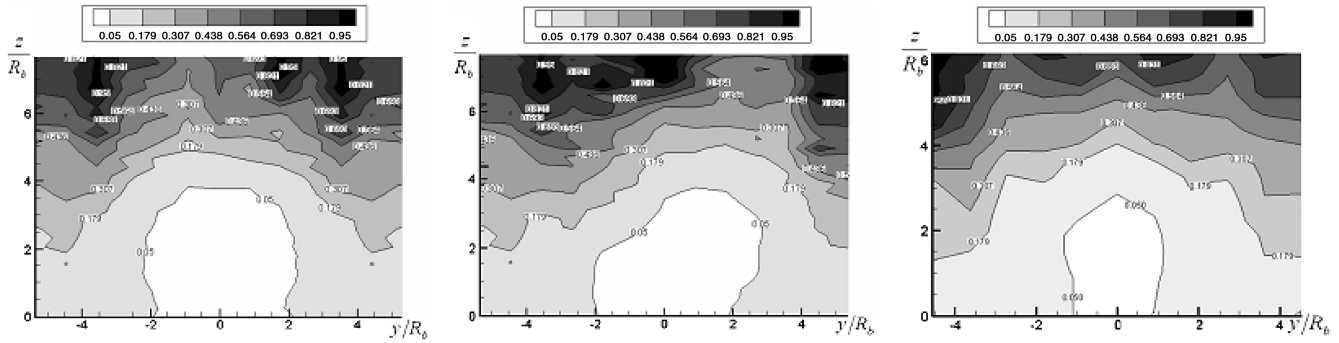

Fig. 7 Normalized total pressure contours $p_t/p_{t,\infty}$ for baseline cases (left), aligned diamond injector (middle), and yawed diamond injector (right) round injector.

pressure loss parameter calculated using a numerical integration of the mass-flow-weighted total pressure field over the sampling plane. The total pressure loss parameter Π is related to the pressure recovery factor $p_{t,\text{rec}}$ as follows [1]:

$$p_{t,\text{rec}} = \frac{\int \rho u p_t \, \mathrm{d}A}{\rho_j u_j p_{t,j} A_j + \int \rho_\infty u_\infty \, \mathrm{d}A} \tag{3}$$

and

$$\Pi = 1 - p_{t,\text{rec}} \tag{4}$$

where ρ is density, u is velocity, p_t is local total pressure, and A is area.

From Eq. (4), a total pressure loss parameter value of $\Pi = 0$ indicates no overall total pressure loss. The results of the total pressure loss parameter calculations can be seen in Table 2. These results show that the diamond injectors generate lower overall pressure losses than the round injector. The aligned diamond shows a total pressure loss parameter of $\Pi = 0.294$ as compared with the round injector total pressure loss parameter of $\Pi = 0.378$, while the yawed diamond injector shows further improvement with a total pressure loss parameter of $\Pi = 0.250$. It is perhaps counterintuitive that the yawed diamond gives a somewhat lower integrated, mass-flow-weighted total pressure loss than the aligned diamond. However, one can see a hint of this result in the shape and size of the contours in Fig. 7. The diamond injectors generate lower overall total pressure losses despite showing higher local pressure losses, because overall total pressure loss is mass-flow averaged. Thus, it is a function not only of local pressure but also of local density and velocity. The round injector generates a higher velocity field near the jet plume than the diamond injectors, because it uses the same mass flow for similar density through a smaller hole.

3. *Mass Fraction Contours and Jet Interaction Parameters*

Figure 8 shows helium mass fraction contours representing the results of the concentration measurements. The magnitude of maximum helium concentration $\alpha_{\max}$ is identified on each plot, and its location in the plume is designated by a × symbol. The minimum isoline $\alpha = 0.028$ represents the a near-stoichiometric value for homogeneous H_2–air combustion at ambient conditions. The centroid of the lean-limit mass fraction contour ($\alpha = 0.003$) [1] is considered the plume center of mass and is marked by a ● symbol in the plots.

The mass fraction contours show that the core of the jet, defined as the location of maximum concentration is located at $(y/R_b, z/R_b) = (-1.79, 2.07)$ for the aligned diamond injector, $(y/R_b, z/R_b) = (0.00, 2.84)$ for the yawed diamond injector, and $(\mathrm{y/R}_b, \mathrm{z/R}_b) = (0.00, 2.48)$ for the round injector. The jet core for all three injectors is within the boundary layer, which has a thickness of $5.65R_b$ at the measurement plane.

Figure 8 indicates that the diamond injectors produce a larger spread of helium with higher penetration (based on the location of the centroid), while the round injector generates more mixing. The two diamond injectors show similar mixing performance, while the yawed diamond injector plume is narrower but with higher penetration. The characteristic dual-lobe structure indicating a counter-rotating vortex pair is evident in the aligned diamond injector and the round injector, but for the yawed diamond injector, the cores are not obvious. Figure 9 shows the two diamond injector mass fraction contours with a larger range of mass fraction isolines to capture the internal structure of the plume core. With the expanded range, the two cores of the vortex pair become visible in the yawed diamond, but one is higher than the other, and they are no longer side by side. This phenomenon is likely due to the addition of span-wise flow generated by the yawed diamond shape. The interaction of the span-wise flow with the vortex pair enhances streamwise vorticity thus increasing jet penetration.

To quantify injector penetration performance, the z-coordinate of the plume center of mass is used. This indicates the penetration of the plume into the supersonic crossflow [1]:

$$z^+ = \frac{\int \rho u \alpha z \, \mathrm{d}A}{\int \rho u \alpha \, \mathrm{d}A} \tag{5}$$

where α is the local helium mass fraction, z is the normalized distance above the tunnel floor, and dA is the differential area. These integrals were evaluated numerically and the results can be found in Table 2,

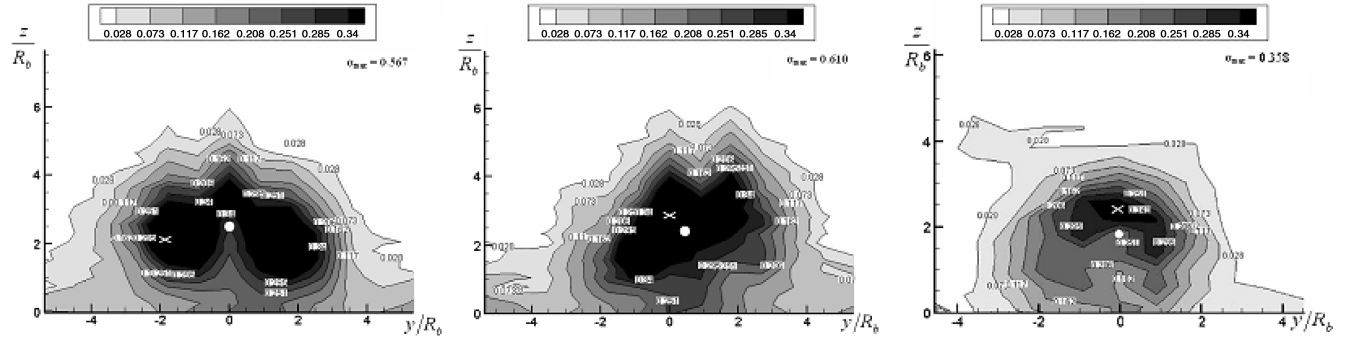

Fig. 8 Mass fraction contours α for baseline cases (left), aligned diamond injector (middle), and yawed diamond injector (right) round injector.

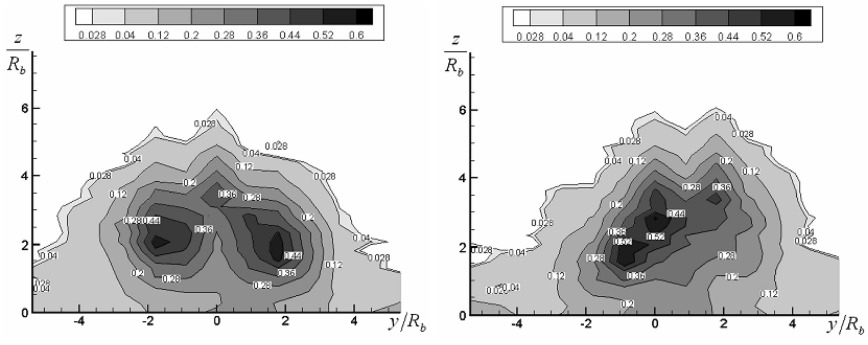

Fig. 9 Mass fraction contours α with expanded range: (left) aligned diamond injector and (right) yawed diamond injector.

Table 2 Baseline injectors plume parameters

Parameter	Aligned diamond injector	Yawed diamond injector	Round injector
z^+	2.30	2.44	1.60
η_m	0.18	0.17	0.20
Π	0.294	0.250	0.378
$y^\pm$	8.5	8.0	6.3

which shows that aligned diamond injector penetrates to a height of $z^+ = 2.30R_b$, which is higher than the round injector penetration of $z^+ = 1.60R_b$. The yawed diamond injector penetrates slightly higher still to a height of $z^+ = 2.44R_b$.

The plume width is defined as the normalized span-wise distance between the stoichiometric edges of the plume. Plume width performance $y^\pm$ is also presented in Table 2. Both diamond injectors generate wider plumes than the round injector, which spreads to a width of $y^\pm = 6.3R_b$. The aligned diamond injector plume is slightly wider with a width of $y^\pm = 8.5R_b$ than the yawed diamond injector, which had a width of $y^\pm = 8.0R_b$.

Because there is no combustion occurring in this nonreacting experiment, it is useful to quantify the mixing performance of the injector to predict the combustion performance in an actual supersonic combustor with the same pressure field. The mixing performance is quantified by a mixing efficiency value η_m defined by the mass-flow rate of fuel, which would theoretically react assuming quasi-one-dimensional, steady isentropic flow over the total mass-flow rate of the fuel as follows [1]:

$$\eta_m = \frac{\int \rho u Z \, \mathrm{d}A}{\int \rho u \alpha \, \mathrm{d}A} \tag{6}$$

where Z is a stoichiometric evaluation of mass fraction as follows:

$$Z = \alpha \quad \text{if } \alpha \le f \qquad Z = \frac{(1-\alpha)f}{(1-f)} \quad \text{if } \alpha > f \tag{7}$$

where f is the stoichiometric combustion mass fraction value. In Eq. (7), $\alpha \le f$ represents the H_2-lean to H_2-consumed case and $\alpha > f$ represents the O_2-lean to O_2-consumed case. Mixing efficiencies are shown in Table 2. The aligned and yawed diamond injectors have similar mixing efficiency values of 0.18 and 0.17, respectively, while the round injector mixes slightly faster with an efficiency value of 0.20.

Table 2 displays all the injector performance parameters for the baseline cases at a measurement plane $15.0R_b$ downstream of the injector orifices. Both diamond injectors show better penetration than the round injector. The aligned diamond injector penetrated 44% higher than the round injector, while the yawed diamond penetrated 53% higher than the round injector. The diamond injectors produce not only higher penetrating plumes, but also wider plumes compared with the round injector. The aligned diamond injector produced a plume 34% wider than the round injector, while the yawed diamond injector produced a 26% wider plume than the round injector.

The mixing efficiencies are nearly identical between the two diamond injectors, and both mix 10–15% slower than the round injector as qualitatively expected from Fig. 8. The results in Table 2 also show that the diamond injectors generate lower overall pressure losses than the round injector. The aligned diamond injector generates 22% lower total pressure loss than the round injector, while the yawed diamond injector generates 34% lower total pressure loss than the round injector.

B. Lower Mass-Flow Cases

This section discusses the total temperature, total pressure, and concentration (mass fraction) data for the injectors using a mass flow of $G_j = 1.5$ g/s corresponding to an effective radius of 2.57 mm. The results for the lower $\bar{q}$ ($\bar{q} = 0.49$) diamond were compared with the lower R_b round injector ($\bar{q} = 1.75$). These conditions correspond to a "well-designed" round injector compared with a well-designed diamond injector. Here, we refer again to the fact that previous studies have shown that diamond and round injectors each perform best at different values of $\bar{q}$. All plots in this section were taken from the measurement plane $22.5R_b$ downstream of the injectors.

1. *Total Temperature Contours*

Figure 10 shows the total temperature contours for the lower mass-flow cases.

The total temperature profiles from both injectors show the dual-lobe structure seen in the baseline cases, which is indicative of the presence of a counter-rotating vortex pair.

The total temperature contour shows a temperature gradient in the round injector profile with lower maximum temperature than the diamond injector. The diamond injector higher temperature lobes indicate that more helium was trapped in the vortex cores. This observation is based on the fact that the helium is heated while the freestream air is cold, thus areas of higher temperature are observed to contain more heated helium.

2. *Total Pressure Contours and Total Pressure Loss Parameter*

Figure 11 shows the total pressure contours for the lower mass-flow cases.

The results of the total pressure loss parameter calculations can be seen in Table 3. These results indicate that the diamond injector generates lower overall total pressure loss than the round injector. The diamond injector shows a total pressure loss parameter of $\Pi = 0.253$ as compared with the round injector, which shows a total pressure loss parameter of $\Pi = 0.373$.

3. *Mass Fraction Contours and Jet Interaction Parameters*

Figure 12 shows helium mass fraction contours representing the results of the concentration measurements for the lower mass-flow case. Again, the magnitude of maximum helium concentration $\alpha_{\max}$ is identified on each plot, and its location is designated by a $\times$ symbol. The centroid of the lean-limit mass fraction ($\alpha = 0.003$) [1] is considered the plume center of mass and is marked by a ● symbol in the plots.

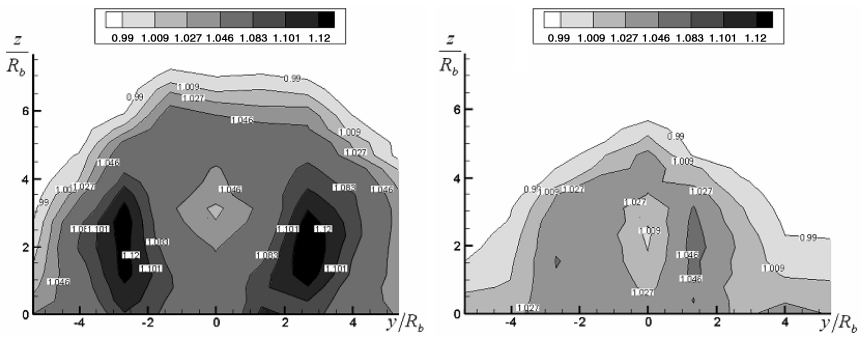

Fig. 10 Normalized total temperature contours $T_t/T_{t,\infty}$ for lower mass-flow cases (left) and diamond injector (right) round injector.

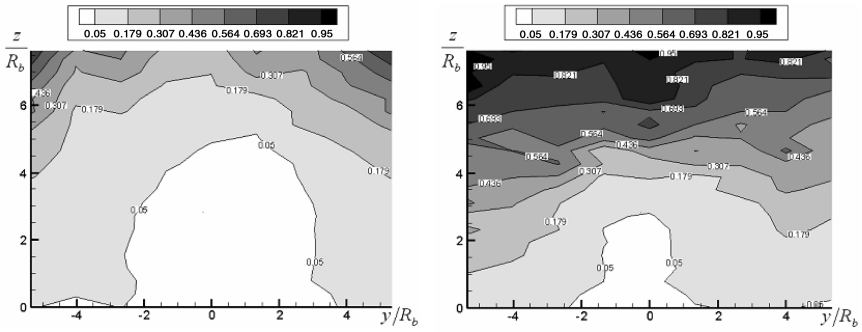

Fig. 11 Normalized total pressure contours $p_t/p_{t,\infty}$ for lower mass-flow cases (left) and diamond injector (right) round injector.

The mass fraction contours show that the core of the jet, defined as the location of maximum concentration is located at $(y/R_b, z/R_b) = (-1.36, 3.12)$ for the diamond injector and $(y/R_b, z/R_b) = (-1.36, 2.33)$ for the round injector. The jet core for both injectors is within the boundary layer which has a thickness of $8.50R_b$ at the measurement plane.

Figure 12 indicates that the diamond injector produces a larger spread of helium with higher penetration than the round injector. The characteristic dual-lobe structure indicating the presence of the counter-rotating vortex pair is evident in the diamond injector profile, while the two cores have merged by the measurement plane in the round injector.

To quantify injector penetration performance, the z coordinate of the plume center of mass is used. The results can be found in Table 3, which shows that the diamond injector penetrates to a height of $z^+ = 3.37R_b$, which is higher than the round injector penetration height of $z^+ = 2.22R_b$. Plume width performance y^+ is also presented in Table 3. The diamond injector generates a wider plume with a width of $y^+ = 10.5R_b$ than the round injector with a plume width of $y^+ = 7.5R_b$.

The mixing performance is quantified as before by a mixing efficiency value η_m. These efficiencies are displayed in Table 3, which shows that the diamond and round injectors have similar mixing efficiency values of 0.26 and 0.27, respectively.

Table 3 displays all the injector performance parameters for the lower mass-flow injectors at a measurement plane $22.5R_b$ downstream of the injector orifices. The diamond injector shows better penetration than the round injector. The aligned diamond injector penetrated 52% higher than the round injector. The diamond injector produces not only a higher penetrating plume, but also a wider plume, 39% wider than the round injector.

The mixing efficiencies are nearly identical between the two injectors with the diamond injector mixing just 4% slower than the round injector. The results presented in Table 3 also show that the diamond injector generates lower overall total pressure loss than the round injector. The diamond injector generates 32% lower total pressure loss than the round injector for the lower mass-flow case.

V. Conclusions

Experiments were conducted to evaluate the performance of different flush-walled fuel injectors for use in scramjet engines. The study focused on 60 deg diamond injectors; 30 deg round injectors were also tested for comparison. The diamond injector was investigated both aligned with the freestream flow and at a yaw angle of 15 deg at the baseline jet-to-freestream momentum flux ratio of $\bar{q} = 1.04$ with a mass flow of $G_j = 3.4$ g/s corresponding to an effective radius of $R_b = 3.54$. The diamond injector was also investigated aligned with the freestream flow at a lower jet-to-freestream momentum flux ratio of $\bar{q} = 0.49$ shown to be optimal at other conditions [13] with a lower mass flow of $G_j = 1.5$ g/s corresponding to an effective radius of $R_b = 2.35$ mm. The round injector investigated at the lower mass-flow condition had a smaller diameter than the round injector at the baseline mass flow to keep the same jet-to-freestream momentum flux ratio of $\bar{q} = 1.75$ for both cases.

Table 3 Lower mass-flow injectors plume parameters

Parameter	Diamond injector	Round injector
z^+	3.37	2.22
η_m	0.26	0.27
Π	0.253	0.373
$y^{\pm}$	10.5	7.5

Helium was used as the injectant to safely simulate hydrogen fuel for real scramjet operation. The investigation was conducted in the Virginia Polytechnic Institute and State University's supersonic wind tunnel with a nominal Mach 4 nozzle to simulate the Mach number seen in the combustor of a scramjet flying at Mach 10. For these experiments, there was a weak oblique shock at the end of the nozzle resulting in a Mach number of $M_\infty = 3.8$, total pressure of $P_{t,\infty} = 1029$ kPa and total temperature of $T_{t,\infty} = 295$ K in the freestream at the injector location.

Profiles of total temperature, total pressure, and helium concentration were generated at measurement planes normal to the freestream flow to qualitatively evaluate the injector performance. The measurement plane was $15.0R_b$ downstream of the injectors for the baseline case and $22.5R_b$ downstream of the injectors for the lower mass-flow case. For quantitative evaluation of injector performance, several performance parameters were used: normalized jet penetration, mixing efficiency, total pressure loss parameter, and normalized plume width.

Conclusions from the investigation can be summarized as follows. For the baseline cases, the aligned diamond injector showed 44% higher penetration than the round injector, while yawing the diamond injector improved penetration to 53% higher than the round injector. The aligned and yawed diamond injectors generated similar mixing efficiencies that were 10 and 15% lower than the round injector, respectively. Yawing the diamond injector also improved the total pressure loss parameter producing a value 34% lower than the round injector as compared with a value 22% lower than the round injector for the aligned diamond injector. The yaw angle was a detriment to the plume width, as the aligned diamond injector produced a 34% wider plume than the round injector, while the yawed diamond only produced a 22% wider plume than the round injector.

For the lower $\bar{q}$ case, the diamond injector showed similar performance to the baseline yawed diamond injector when compared with their respective round injectors, which showed a 53% penetration increase. The lower $\bar{q}$ diamond injector improved to nearly the same mixing efficiency as the round injector with just a 4% lower value. The lower $\bar{q}$ diamond injector showed similar total pressure loss to the baseline yawed diamond injector with a total pressure loss parameter 32% lower than the round injector. The lower $\bar{q}$ showed an improved plume width over both the baseline diamond injectors with a 39% wider plume than the round injector. The lower $\bar{q}$ cases were selected to compare a well-designed diamond injector to a well-designed round injector. The present results confirm the conclusions of earlier, lower freestream Mach number and higher molecular weight injectant studies that a slender diamond injector provides significant benefits for crossflow penetration and lower total pressure losses.

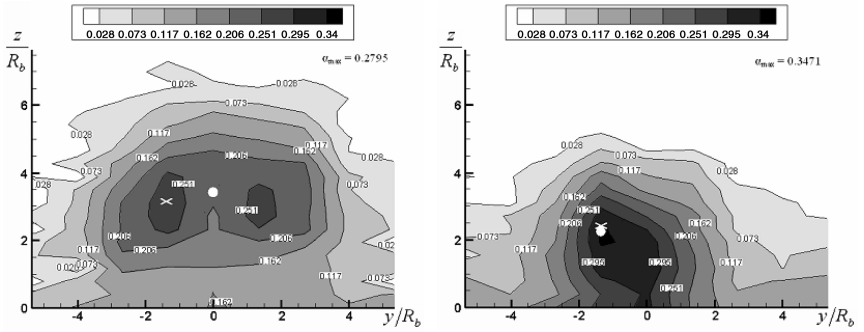

Fig. 12 Mass fraction contours α for lower mass-flow cases (left) and diamond injector (right) round injector.

Further investigations of the diamond injectors could include the following. A yawed case at the lower $\bar{q}$ flow conditions could be conducted to determine if the same trends hold as in the baseline case. The measurement plane could be shifted forward and aft in both cases to investigate how the plumes develop as they move downstream of the injector. Finally, testing at hot-flow freestream conditions could be investigated to simulate the flow in a real scramjet case.

References

[1] Maddalena, L., Campioli, T. L., and Schetz, J. A., "Experimental and Computational Investigation of an Aeroramp Injector in a Mach Four Cross Flow," AIAA Paper 2005-3235, June 2005.

[2] Hartfield, R. J., Hollo, S. D., and McDaniel, J. C., "Experimental Investigations of a Supersonic Swept Ramp Injector Using Laser Induced Iodine Fluorescence," *Journal of Propulsion and Power*, Vol. 10, No. 1, Jan.–Feb. 1994, pp. 129–135.

[3] Doerner, S. E., and Cutler, A. D., "Effects of Jet Swirl on Mixing of a Light Gas Jet in a Supersonic Airstream," NASA CR-1999-209842, Dec. 1999.

[4] Schetz, J. A., Cox-Stouffer, S., and Fuller, R., "Integrated CFD and Experimental Studies of Complex Injectors in Supersonic Flows," AIAA Paper 98-2780, June 1998.

[5] Jacobsen, L. S., Gallimore, S. D., Schetz, J. A., and O'Brien, W. F., "Integration of an Aeroramp Injector/Plasma Igniter for Hydrocarbon Scramjets," *Journal of Propulsion and Power*, Vol. 19, No. 2, March–April 2003, pp. 170–182.

[6] Fuller, R. P., Wu, P. K., Nejad, A. S., and Schetz, J. A., "Comparison of Physical and Aerodynamic Ramps as Fuel Injectors in Supersonic Flow," *Journal of Propulsion and Power*, Vol. 14, No. 2, March–April 1998, pp. 135–145.

[7] Jacobsen, L. S., Gallimore, S. D., Schetz, J. A., O'Brien, W. F., and Goss, L. P., "Improved Aerodynamic-Ramp Injector in Supersonic Flow," *Journal of Propulsion and Power*, Vol. 19, No. 4, July–Aug. 2003, pp. 663–674.

[8] Viti, V., Schetz, J. A., and Neel, R., "Numerical Studies of the Jet Interaction Flowfield with a Main Jet and an Array of Smaller Jets," ICAS Paper 2002-4.7.1, 2002.

[9] Schetz, J. A., Cox-Stouffer, S., and Fuller, R., "Integrated CFD and Experimental Studies of Complex Injectors in Supersonic Flows," AIAA Paper 98-2780, 1998.

[10] Riggins, D. W., and Vitt, P. H., "Vortex Generation and Mixing in Three-Dimensional Supersonic Combustors," *Journal of Propulsion and Power*, Vol. 11, No. 3, May–June 1995, pp. 419–426.

[11] Lewis, D. P., and Schetz, J. A., "Tangential Injection from Overlaid Slots into a Supersonic Stream," *Journal of Propulsion and Power*, Vol. 13, No. 1, Jan.–Feb. 1997, pp. 59–63.

[12] Schetz, J. A., Billig, F. S., Favin, S., and Gilreath, H. E., "Effects of Pressure Mismatch on Slot Injection in a Supersonic Flow," *International Journal of Turbo and Jet Engines*, Vol. 9, No. 2, 1992, pp. 135–146.

[13] Tomioka, S., Jacobsen, L. S., and Schetz, J. A., "Sonic Injection from Diamond-Shaped Orifices into a Supersonic Crossflow," *Journal of Propulsion and Power*, Vol. 19, No. 1, Jan.–Feb. 2003, pp. 104–114.

[14] Barber, M. J., Schetz, J. A., and Roe, L. A., "Normal Sonic Helium Injection Through a Wedge-Shaped Orifice into a Supersonic Flow," *Journal of Propulsion and Power*, Vol. 13, No. 2, March–April 1997, pp. 257–263.

[15] Schetz, J. A., "Interaction Shock Shape for Transverse Injection," *Journal of Spacecraft and Rockets*, Vol. 7, No. 2, Feb. 1970, pp. 143–149.

[16] Fuller, E. J., Mays, R. B., Thomas, R. H., and Schetz, J. A., "Mixing Studies of Helium in Air at Mach 6," AIAA Paper 91-2268, June 1991.

[17] McClinton, C. R., "The Effect of Injection Angle on the Interaction Between Sonic Secondary Jets and a Supersonic Freestream," NASA TND-6669, Feb. 1972.

[18] Rogers, R. C., "A Study of the Mixing of Hydrogen Injected Normal to a Supersonic Airstream," NASA TN L-7386, Langley Research Center, March 1971.

[19] Jacobsen, L. J., Schetz, J. A., Gallimore, S. D., and O'Brian, W. F., "Mixing Enhancement by Jet Swirl in a Multiport Injector Array in Supersonic Flow," FEDSM Paper 99-7448, July 1999.

[20] Kraus, D. K., and Cutler, A. D., "Mixing of Swirling Jets in a Supersonic Duct Flow," *Journal of Propulsion and Power*, Vol. 12, No. 1, Jan.–Feb. 1996, pp. 170–177.

[21] Cutler, A. D., and Johnson, C. H., "The Use of Swirling Jet Pairs to Provide Rapid Fuel Penetration in Scramjet Combustors," AIAA Paper 95-0099, 1995.

[22] Schetz, J. A., *Injection and Mixing in a Turbulent Flow*, AIAA, New York, 1980.

[23] Povinelli, L. A., and Ehlers, R. C., "Swirling Base Injection for Supersonic Combustion Ramjets," *AIAA Journal*, Vol. 10, No. 9, Sept. 1972, pp. 1243–1244.

[24] Schetz, J. A., and Swanson, R. C., "Turbulent Jet Mixing at High Supersonic Speeds," *Zeitschrift für Flugwissenschaften*, Vol. 21, 1973, pp. 166–173.

[25] Schetz, J. A., Thomas, R. H., and Billig, F. S., "Mixing of Transverse Jets and Wall Jets in Supersonic Flow," *Separated Flows and Jets*, edited by V. V. Kozlov and A. V. Dovgal, Springer–Verlag, Berlin, 1991.

[26] Marzouk, Y. M., and Ghoniem, A. F., "Mechanism of Streamwise Vorticity Formation in Transverse Jets," AIAA Paper 2002-1063, Jan. 2002.

[27] Ng, W. F., Kwok, F. T., and Ninnemann, T. A., "A Concentration Probe for the Study of Mixing in Supersonic Shear Flows," AIAA Paper 89-2459, July 1989.

[28] Grossman, P., "Experimental Investigation of a Flush-Walled, Diamond-Shaped Fuel Injector for High Mach Number Scramjets," M.S. Thesis, Virginia Polytechnic Institute and State University, Blacksburg, VA, Dec. 2006.

J. Oefelein
Associate Editor